BIOCHEMISTRY
including biophysical chemistry & molecular biology

Article

pubs.acs.org/biochemistry

Identification of Structural−Kinetic and Structural−Thermodynamic Relationships for Thrombin Inhibitors

Johan Winquist,[†] Stefan Geschwindner,[§] Yafeng Xue,[§] Lars Gustavsson,[‡] Djordje Musil,[‡,∥] Johanna Deinum,[‡] and U. Helena Danielson*[,†]

[†]Department of Chemistry−BMC, Uppsala University, SE-751 23 Uppsala, Sweden

[‡]CVGI iMED, AstraZeneca, SE-431 83 Mölndal, Sweden

[§]Discovery Sciences, AstraZeneca R&D Mölndal, SE-431 83 Mölndal, Sweden

Supporting Information

ABSTRACT: To improve our understanding of drug−target interactions, we explored the effect of introducing substituted amine residues with increased chain length in the P3 residue of the thrombin inhibitor melagatran. Inhibition, kinetic, and thermodynamic data obtained via stopped-flow spectroscopy (SF), isothermal microcalorimetry (ITC), and surface plasmon resonance (SPR) biosensor analysis were interpreted with the help of X-ray crystal structures of the enzyme−inhibitor complexes. The association rate became faster when the lipophilicity of the inhibitors was increased. This was coupled to an increased enthalpic component and a corresponding decreased entropic component. The dissociation rates were reduced with an increase in chain length, with only a smaller increase and a decrease in the enthalpic and entropic components, respectively. Overall, the affinity increased with an increase in chain length, with similar changes in the enthalpic and entropic components. ITC analysis confirmed the equilibrium data from SPR analysis, showing that the interaction of melagatran was the most enthalpy-driven interaction. Structural analysis of the thrombin−inhibitor complex showed that the orientation of the P1 and P2 parts of the molecules was very similar, but that there were significant differences in the interaction between the terminal part of the P3 side chain and the binding pocket. A combination of charge repulsion, H-bonds, and hydrophobic interactions could be used to explain the observed kinetic and thermodynamic profiles for the ligands. In conclusion, changes in the structure of a lead compound can have significant effects on its interaction with the target that translate directly into kinetic and thermodynamic effects. In contrast to what may be intuitively expected, hydrogen bond formation and breakage are not necessarily reflected in enthalpy gains and losses, respectively.

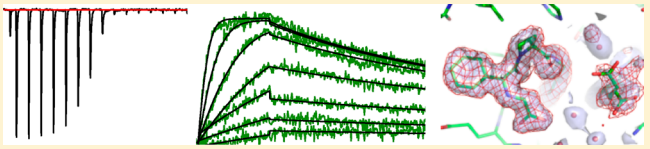

Drug discovery is a complex, multivariate process in which optimal characteristics of a lead compound influencing its interaction with its target are balanced with respect to other properties, such as adsorption, distribution, metabolism, excretion, and toxicology (ADMET). However, the ideal properties of a drug are not known *a priori* but need to be established by correlating biochemical features with physiological efficacy in a lengthy and typically serial process. A number of metrics focusing on the characteristics of the compounds as such, e.g., the Lipinski rule of five, have emerged and are now used for prioritizing hits and leads. These simple metrics have more recently been complemented by presumed favorable interaction characteristics, for example, the rather intuitive advantage of slow dissociation of a drug from its target, which translates into a long residence time.[1] This has resulted in an awareness of the importance of determining the kinetics of lead−target interactions. Similarly, the thermodynamics of lead−target interactions have become of interest. Despite the more elusive understanding of the entropy and enthalpy of binding, high-affinity interaction is expected to have favorable contributions of both these parameters. However, it appears that standard medicinal chemistry procedures for lead optimization may inadvertently result in compounds with a dominating entropic contribution to affinity, because high-throughput screening seldom can provide values other than equilibrium values.[2] Because binding enthalpy appears to be more difficult to optimize than binding entropy, the current focus is on identifying hit and lead compounds that are enthalpy-dominated. Although kinetic and thermodynamic parameters provide a means of identifying and prioritizing hit and lead compounds, the ideal characteristics have been compiled from retrospective analyses of drugs in the clinic rather than a systematic analysis of the correlation between these properties and clinical efficacy. Moreover, the chemical basis and general validity of these rules remain to be established. In this study, we have therefore focused on exploring how interaction kinetics and thermodynamics for a relevant drug−target system can be reliably established and interpreted in a structural context.

Thrombin (EC 3.4.21.5) is a key enzyme in the blood clotting cascade and an important target for anticoagulant

Received: September 30, 2012
Revised: December 21, 2012
Published: January 4, 2013

dx.doi.org/10.1021/bi301333z | *Biochemistry* 2013, 52, 613−626

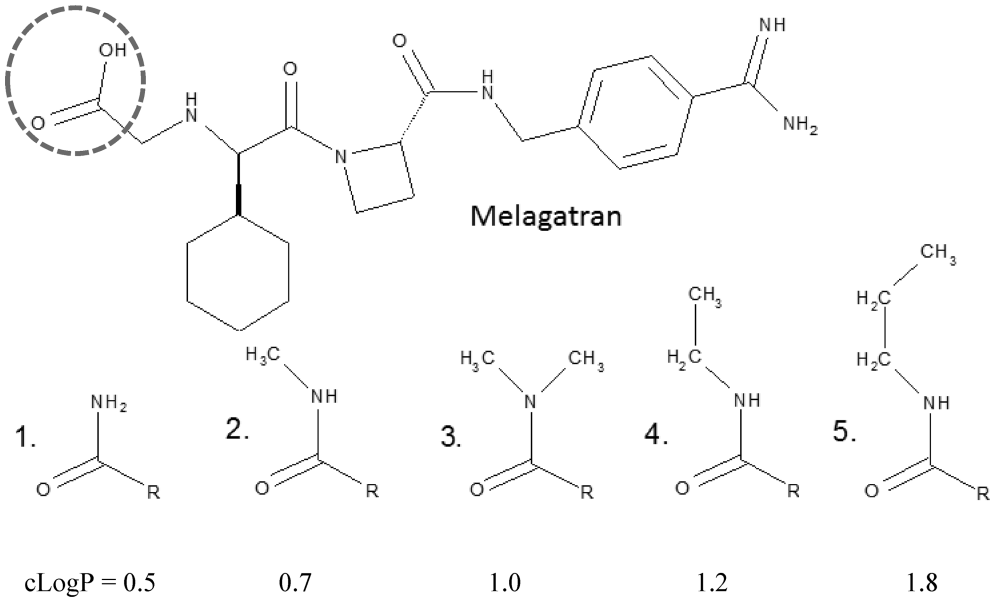

Figure 1. Melagatran and the five P3 side chain analogues studied. The terminal part of the P3 side chain (circled) was substituted with groups **1**−**5**. Groups **2**, **4**, and **5** exist mostly in the trans configuration. cLogP values for compounds **1**−**5** are given below each structure.

drugs, preventing thromboembolism and stroke. Thrombin specifically cuts fibrinopeptides from fibrinogen to yield fibrin and activates the thrombin receptor, e.g., in platelets. Structurally, the catalytic triad of thrombin is located at the interface between the two main β-sheet domains of the protein. Unlike many other serine proteases, thrombin is highly selective and cleaves between P1 and P1′ in the consensus recognition sequence[3] P2-Pro, P1-Arg, P1′-Ser/Ala/Gly/Thr, P2′-not acidic, and P3′-Arg (the nomenclature of Schechter and Berger[4] is used here for defining the substructures of the inhibitors and their binding sites in the protein). The high substrate selectivity is obtained as a result of an unusually deep and narrow active site cleft with an aspartic acid residue positioned in the bottom of the S1 pocket, forming a salt bridge with the P1 residue of the substrate. The S2 subsite created by Tyr60A and Trp60D of the thrombin-specific insertion loop as well as Cys99 and Met57 is a hydrophobic cavity that can harbor smaller to medium-sized hydrophobic residues, such as proline. The S4 aryl binding site, as defined by Leu99, Trp215, and Ile174, is smaller and more hydrophobic in thrombin than in the trypsin counterpart, which also contributes to the high selectivity of thrombin relative that of trypsin and many other enzymes in this class of serine proteases.

Thrombin has been well characterized as a drug target, and what it takes for a thrombin inhibitor to be effective is known; as for many drugs, it must bind with high affinity, i.e., have a low K_i value, in combination with fast formation of the enzyme−inhibitor complex, i.e., a high k_{on} value.[5,6] Melagatran is an active site α-thrombin inhibitor that fulfils these criteria and has been used in the clinic, as the prodrug ximelagatran. Unfortunately, it had to be removed from the market because of reported liver injury. However, it still represents an interesting compound from which we can learn much about how to identify and optimize lead compounds. A basic understanding of the interaction between melagatran and thrombin has previously been described,[7−11] as has the contribution of a variety of P2−P3 moieties.[12,13] In more detail, it appears that the electrostatic interaction between the charged P1 residue and the S1 site contributes to a rapid binding of melagatran, while additional stabilization of the complex is achieved via hydrophobic interactions between the P3 residue and the S3 site. However, the finer kinetic and thermodynamic details as well as the interpretation within a structural context are lacking.

To identify the structural features of the ligands and the target that influence the formation and breakup of the ligand−target complex, and the consequences of these structural determinants with respect to inhibition, interaction kinetics, and thermodynamics, we have here used melagatran and thrombin as a relevant model system. A series of melagatran analogues with the hydroxyl group in the P3 carboxyl group replaced with amine residues of increasing chain length and hydrophobicity were selected (Figure 1). The compounds are examples of inhibitors that had evolved during lead optimization but not progressed to clinical studies. A combination of complementary experimental techniques was adopted to gain a sufficiently detailed understanding of the interaction between the inhibitors and thrombin. Kinetic and thermodynamic data were obtained via stopped-flow spectroscopy (SF), isothermal microcalorimetry (ITC), and surface plasmon resonance (SPR) biosensor technology, three methods with different experimental designs and readouts that provide overlapping information. Structural data for the ligand−target complexes were obtained by X-ray crystallography. The data provided a solid foundation for the interpretation of the effect of structural changes in a ligand on its kinetic and thermodynamic properties, at least for the P3 analogues of melagatran.

MATERIALS AND METHODS

Enzyme and Inhibitors. For the stopped-flow experiments, a 4 μM stock solution of α-thrombin (Sigma-Aldrich, St. Louis, MO) was prepared in 50 mM 2-[4-(2-hydroxyethyl)-1-piperazinyl]ethanesulfonic acid (HEPES) with 100 mM NaCl and 0.1% (w/v) PEG6000. The concentration of α-thrombin was determined by absorbance spectroscopy using an ε_{280} of 66.8 mM^{-1} cm^{-1},[14] while the specific activity was 84%, as

dx.doi.org/10.1021/bi301333z | *Biochemistry* 2013, 52, 613−626

determined by active site titration with recombinant leech hirudin (Sigma), essentially as described previously.[15]

For the biosensor, ITC, and crystallization experiments, α-thrombin was prepared from lyophilized plasma-derived human prothrombin (Enzyme Research Laboratories, South Bend, IN) via digestion with ecarin, prepared from the venom of *Echis carinatus* (DSM Nutritional Products Ltd. Branch Pentapharm, Basel, Switzerland), following a protocol that was developed for process scale applications. In short, prothrombin (1 mg/mL) was incubated with ecarin (0.04 unit/mL) for 4 h at 37 °C in PBS [4.3 mM Na_2HPO_4, 1.47 mM KH_2PO_4, 2.7 mM KCl, and 137 mM NaCl (pH 7.4)]. The conductivity and pH of the reaction mixture were adjusted to 10 mS/cm and 6.5, respectively, prior to it being subjected to an ion-exchange chromatography step using a HiTrap SP HP column (GE Healthcare, Uppsala, Sweden) with a column volume of 5 mL. Tween-80 was added to a final concentration of 0.1% (w/w) to remove aggregated protein. After sample application and equilibration with 50 mM Na_2HPO_4 (pH 6.5), the protein was eluted via a step elution, using 350 mM NaCl in the same buffer. For the final purification, the pooled fractions from the elution were adjusted with 5 M NaCl to a conductivity of ∼180 mS/cm and applied to a HiTrap Butyl FF column (GE Healthcare) with a column volume of 5 mL. After equilibration with 50 mM Na_2HPO_4 and 3 M NaCl (pH 6.5), the protein was eluted via a step gradient using 50 mM Na_2HPO_4 (pH 6.5).

The thrombin inhibitors were synthesized according to published procedures.[9] The logarithm of the partition coefficient between *n*-octanol and water, $\log(c_{octanol}/c_{water})$, for the compounds (cLogP) was calculated for the compounds using ISIS Base and ISIS Draw 2.1.3d (MDL Information Systems Inc., San Leandro, CA) using an algorithm provided by ACD/Lab Programs (Toronto, ON).[16] For the ITC experiments, the concentration of melagatran was determined by NMR. It could thereby serve as a reliable reference, confirming the activity state and ligand binding competence of the protein.

Enzyme Kinetic Analysis. The chromogenic substrate, H-D-phenylalanyl-L-pipecolyl-L-arginine-*p*-nitroaniline dihydrochloride (Chromogenix, Mölndal, Sweden), was dissolved in water to a final concentration of 40 mM. For K_m determinations, it was further diluted to 100 μM with assay buffer [50 mM HEPES, 150 mM NaCl, and 0.1% (w/v) bovine serum albumin (BSA, fraction V, ICN Biomedicals, Aurora, OH) (pH 7.21)]. A separate solution was prepared for each temperature. The pH was corrected at room temperature with 1.0 M NaOH or 1.0 M HCl to yield the theoretically correct pH value for each buffer solution calculated using a value of 7.52 for the apparent pK_a and a temperature coefficient of −0.014 $°C^{-1}$ for HEPES.[17] All solutions were filtered through a 0.2 μm sterile Acrodisc filter (Gelman Science, Ann Arbor, MI) and degassed for 15 min in an ultrasonic bath. Product formation was measured at 405 nm, using an ε_{405} of 9920 M^{-1} cm^{-1}.[18]

Initial Rate Analysis. The k_{cat} and K_m values for the chromogenic substrate and thrombin were determined from initial rates at 17, 24, 30, 34, and 37 °C, using 1.0−50 μM substrate and 0.82 nM thrombin in assay buffer. Analysis was performed with a Roche Cobas Bio centrifugal analyzer (F. Hoffmann-La Roche & Co. Ltd., Basel, Switzerland) for 3 min. Nonlinear regression analysis using the Michaelis−Menten equation was performed with GraFit (Erithacus Software Ltd., Staines, U.K.).

Pre-Steady-State Analysis. Pre-steady-state kinetic analysis of thrombin activity was performed with an SF-61 DX2 stopped-flow apparatus (Hi-Tech Scientific Ltd., Salisbury, U.K.). It was used in the single-mixing mode with a dead time of approximately 4 ms, depending on the air pressure used. KinetAsyst2 (Hi-Tech) was used for data analysis. Equal parts of a solution containing 8.2 nM human α-thrombin and a solution containing 1.2 mM substrate and inhibitor were mixed. The progress curve data were acquired on a logarithmic time base, with a total of 640 data points in each curve and three to six replicates for each series. Progress curves were analyzed by nonlinear regression (GraFit) using the integrated rate equation:

$$P_t = P_0 + v_s t + (v_0 - v_s)[1 - \exp(-k_{obs} t)]/k_{obs} \quad (1)$$

where P_t and P_0 are the product concentrations at time t and 0, respectively, v_0 is the initial velocity, v_s is the steady-state velocity, and k_{obs} is the apparent first-order rate constant for the establishment of equilibrium in the reaction. The four parameters P_0, v_0, v_s, and k_{obs} were determined from the average progress curves for each inhibitor concentration. By assuming that the rate-limiting step is the attainment of equilibrium between the enzyme and the enzyme−inhibitor complex, we obtained the apparent rate constants (k_{on} and k_{off}) from k_{obs}:

$$k_{obs} = k_{off} + k_{on}[I]/(1 + [S]/K_m) \quad (2)$$

The observation time period was adapted for each individual inhibitor and temperature to establish the steady state during the time period of the progress curve. The inhibition constant, K_i, was calculated from the rate constants:

$$K_i = k_{off}/k_{on} \quad (3)$$

K_i was also determined from IC_{50} values, obtained by steady-state velocities, v_s, for a series of inhibitor concentrations, and by assuming competitive inhibition:

$$v_s = v_0/(1 + [I]/IC_{50}) \quad (4)$$

$$K_{i(st.st)} = IC_{50}/(1 + [S]/K_m) \quad (5)$$

ITC Analysis. Isothermal titration calorimetry experiments were conducted on a MicroCal ITC-200 system (GE Healthcare) using α-thrombin that had been passed through a PD-10 column (GE Healthcare) equilibrated with 10 mM HEPES (pH 7.4), 150 mM NaCl, 0.1% PEG6000, and 1% DMSO. Complete titration of 21−29 μM α-thrombin was typically achieved by injecting 16 × 1.4 μL aliquots of 0.5 mM melagatran or P3-substituted analogues in a temperature interval ranging from 20 to 35 °C.

The thermodynamic binding parameters were extracted by nonlinear regression analysis of the binding isotherms (Microcal Origin version 7.0). A single-site binding model was applied, yielding the binding enthalpy (ΔH), stoichiometry (n), entropy (ΔS), and association constant (K_a). To ensure that the observed binding enthalpy was not perturbed by a net proton release or uptake upon ligand binding and thus dependent on the used buffer system, control titrations in phosphate buffer were also performed. The enthalpies were essentially the same as those obtained in HEPES buffer (data not shown). Even though it is well established that thrombin shows a change in protonation at pH 7.4 at His57, this is compensated by melagatran through simultaneously picking up a proton via its basic nitrogen upon binding. Because of this cancellation, a

relative comparison of the inhibitors across the entire series was possible.

It was not possible to rely on the values for the association constant K_a because the errors in the determination were very large, due to the high c value (>1000) caused by the experimental setup and the high affinity of the tested ligands. The heat capacity change, ΔC_p, was estimated from the temperature dependence of the observed change in enthalpy ($\Delta H/\Delta T$).

SPR Biosensor Analysis. A Biacore S51 SPR-biosensor (GE Healthcare) was used for the analysis of the direct interaction between the inhibitors and immobilized thrombin.

Immobilization of Thrombin. Thrombin [in 10 mM sodium acetate (pH 5.0)] was immobilized on a CM5 biosensor chip (GE Healthcare) by amine coupling (Biacore Handbook, GE Healthcare), essentially as described previously.[8,19] With 10 mM phosphate buffer (pH 7.4), 2.7 mM KCl, 0.14 M NaCl, and 0.05% Tween 20 (PBS-P) as the continuous flow buffer, a mixture of 1-ethyl-3-[3-(dimethylamino)propyl]carbodiimide hydrochloride (EDC) and *N*-hydroxysuccinimide (NHS) was injected over the surface for 7 min, followed by injection of thrombin. Any reactive groups still present on the surface were deactivated by a 7 min injection of 0.1 M ethanolamine hydrochloride-NaOH (pH 8.5).

Interaction Analysis. The interaction analysis was performed in a running buffer (RB) consisting of 50 mM HEPES (pH 7.4), 150 mM NaCl, 3.4 mM EDTA, 0.05% (v/v) Tween 20, and 5% (v/v) DMSO, with a system flow rate of 90 μL/min at seven temperatures (5, 10, 15, 25, 35, 40, and 45 °C). Samples diluted in RB to 0.78, 1.56, 3.13, 6.25, 12.5, 25, and 50 nM were injected for 120 s over the immobilized thrombin and reference surfaces along with blank samples. After dissociation for 600 s, the detector surfaces were regenerated by a 20 s pulse of 100 mM sodium acetate (pH 4.5) with 4 M $MgCl_2$, followed by a 30 s stabilization period.

Data Analysis. To adjust for buffer-deduced signal differences between the thrombin and reference surfaces (because of partial coverage of the sensor surface by immobilized enzyme only on the thrombin surface), an eight-point DMSO solvent correction procedure was used. A nonimmobilized surface and blank samples (negative control) were used for referencing. Kinetic rate constants and the equilibrium dissociation constant were estimated from sensorgrams by global nonlinear regression using a 1:1 Langmuir interaction model (Scheme 1).

$$\mathrm{E} + \mathrm{I} \underset{k_{off}}{\overset{k_{on}}{\rightleftharpoons}} \mathrm{EI} \qquad \text{(Scheme 1)}$$

To identify and exclude mass transport (MT) limited data, the ratio (R_a) of k_{on} times the calculated maximal response (R_{max}) to the mass transport coefficient (k_t) was calculated according to

$$R_a = (k_{on}R_{max})/k_t \qquad (6)$$

Experiments with an R_a of >5 suggest that kinetic rate constants may be unreliable because of MT, although affinities extracted from these experiments may still be valid.[20] Because only the trends of the data were sought, a less stringent upper threshold of 10 was used.

Estimation of Thermodynamic Parameters. Thermodynamic parameters were extracted from equilibrium (K_D) and rate constants (k_{off} and k_{on}) determined over a series of temperatures using SF[7] and SPR data.[21,22] Because this procedure has inherent methodological limitations,[23] the interpretation is focused on the different thermodynamic profiles of the inhibitors. These can be extracted even if the magnitude and accuracy of the thermodynamic parameters are uncertain.

van't Hoff Analysis. van't Hoff analysis was used to estimate the enthalpy (ΔH) and entropy (ΔS) of binding by linear regression analysis from K_D values determined at different temperatures:

$$\ln K_D = -\Delta H/(RT) + \Delta S/R \qquad (7)$$

where R is the gas constant and T the absolute temperature. The analysis assumes a temperature-independent heat capacity, C_p, at a constant pressure.

Arrhenius Analysis. Arrhenius analysis was used to determine the activation energy (E_a) and the pre-exponential factor (A) for the rate constants in the association and dissociation phases separately by linear regression analysis, using k_{off} and k_{on} determined over a series of temperatures:

$$k = Ae^{-E_a/RT} \qquad (8)$$

In the Arrhenius plot [i.e., the natural logarithms of the rate constants (k_{off} and k_{on}) for the inhibitors vs $1/T$], A denotes the intercept while E_a corresponds to the slope of the straight line.

The enthalpies and entropies for the rate constants ($\Delta H^{\ddagger}$ and $\Delta S^{\ddagger}$, respectively) were also determined, through an Arrhenius–Eyring hybrid analysis (see below). The enthalpy of activation was calculated from E_a:

$$\Delta H^{\ddagger} = E_a - RT \qquad (9)$$

while the entropy of activation was estimated from A:

$$A = (Tk_Be^1/h)e^{\Delta S^{\ddagger}/R} \qquad (10)$$

where k_B is Boltzmann's constant and h Planck's constant.

Eyring Analysis. Eyring analysis was used to estimate the thermodynamic parameters for the association and dissociation events from the rate constants by linear regression, using an approach similar to van't Hoff analysis of equilibrium constants:

$$\ln\left(k_{on}\frac{Ch}{k_BT\kappa}\right) = -\frac{\Delta H^{\ddagger}_{on}}{RT} + \frac{\Delta S^{\ddagger}_{on}}{R} \qquad (11)$$

$$\ln\left(k_{off}\frac{h}{k_BT\kappa}\right) = -\frac{\Delta H^{\ddagger}_{off}}{RT} + \frac{\Delta S^{\ddagger}_{off}}{R} \qquad (12)$$

where C is the state of the solvent and κ is the transmission coefficient, both set to 1.

Crystallization and X-ray Structure Determination. Preformed thrombin–hirudin complexes were crystallized, and compounds were soaked into the crystals as previously described.[24] The diffraction data were collected from frozen crystals on a MarResearch 345 mm image-plate detector system mounted on a Rigaku RU300HB rotating anode (Cu Kα radiation, wavelength of 1.54 Å). The crystal-to-detector distance was set to 150 or 160 mm, and diffraction images were collected with 1° oscillation. The data were processed with XDS[25] and programs in the CCP4 suite.[26] Refinement and model rebuilding were conducted using AutoBuster[27] and COOT.[28]

dx.doi.org/10.1021/bi301333z | *Biochemistry* 2013, 52, 613–626

RESULTS

Stopped-Flow Analysis. *Kinetic Analysis.* The inhibition and thermodynamic parameters for the interaction between melagatran and the five P3 analogues (Figure 1) were initially assessed by stopped-flow (SF) analysis. For this, it was first necessary to determine the K_m for the catalytic reaction at the same temperature and under the same conditions that were used for the experiments. Both k_{cat} and K_m were determined by steady-state analysis (see the Supporting Information for data). k_{obs}, k_{on}, k_{off}, and the corresponding inhibition constants (K_i) could then be determined from the progress curves, using nonlinear regression analysis and eq 1 (see the Supporting Information for data). This was done at 17, 24, 30, and 37 °C, so that the data could later be used for the thermodynamic analysis (see below). Because the compounds are active site inhibitors, the analysis was based on a procedure for competitive inhibition (Scheme 1). This procedure was verified to be sound as no hyperbolic residual trends for the k_{obs} values were detected.

Although there were relatively small differences in the inhibitory potencies of the compounds, with K_i values ranging from 1 to 4 nM at 37 °C, some trends could be discerned. The degree of substitution of the amide was clearly a factor, with the K_i for the tertiary amide (compound **3**; K_i = 1.14 ± 0.02 nM) being more than 4 times lower than that for the primary amide (compound **1**; K_i = 4.29 ± 0.10 nM) and approximately half of that for the secondary amide (compound **2**; K_i = 2.43 ± 0.07 nM) (all at 37 °C). Also the length of the alkyl chain had an effect, with the K_i value decreasing until the length was equal to two carbon atoms, i.e., the ethyl substituent. When the alkyl chain was longer or shorter than two carbon atoms, i.e., for the propyl substituent or the methyl substituent, respectively, the K_i value was increased.

However, when the kinetic rate constants were also used for the analysis, as illustrated in the interaction kinetic plot [k_{on} vs k_{off} (Figure 2)] for the data determined at 37 °C, it was clear that there is no simple relationship between kinetic rate constants or K_i values and the lipophilicity or other structural features of the P3 side chains. In fact, it appears that the association rates of the compounds may have reached an upper limit, defined by diffusion, as we also concluded from the SPR biosensor data (see below).

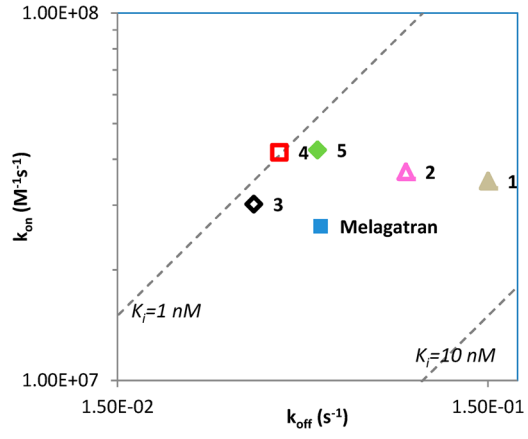

Figure 2. Kinetic rate constants and inhibition constants for melagatran and analogues at 37 °C determined by stopped-flow progress curve analysis (the values and errors are presented in the Supporting Information). The diagonals represent the iso-affinity lines.

Thermodynamic Analysis. The temperature series data were used for estimation of the thermodynamic parameters of the interaction (see the Supporting Information for the graphical analysis and the data set for 25 °C). The thermodynamic analysis of association data from the SF data is less reliable than of dissociation data because the calculation of the k_{on} value is indirect and dependent on the K_m and the substrate and ligand concentrations. It was seen as an unsatisfactory Arrhenius plot for k_{on} and standard deviations of >10% for the estimated thermodynamic parameters. In contrast, thermodynamic analysis of k_{off} data was more reliable, as judged by the essentially linear Arrhenius plots in the studied temperature range. Because of the relatively small temperature range (290–310 K), also the equilibrium data calculated from the $K_i = k_{off}/k_{on}$ relationship were uncertain because a small divergence in the slope factor gives rise to a relatively large difference in ΔH (see Table S3 of the Supporting Information). However, the steady-state data provided similar values for $K_{i(st.st)}$ as calculated for K_i (not shown).

Despite these uncertainties, the data show that the interaction between the inhibitors and thrombin is enthalpy-driven, in both association and dissociation (Figure 3). For k_{on}, a compensatory enthalpy–entropy effect, or isokinetic correlation (see Figure S4 of the Supporting Information), was detected.

Biosensor-Based Interaction Analysis. SPR biosensor technology was used as an alternative approach to determine kinetic and thermodynamic data from kinetic and equilibrium data at several temperatures. An advantage is that it is a direct time-resolved method for analysis of the interaction between the inhibitors and thrombin and does not require substrate conversion, as an enzyme activity-based assay does, such as SF analysis.

Because of the very rapid interaction between the inhibitors and thrombin, low levels of thrombin were immobilized to avoid limited mass transport of ligand into the sensor matrix. A final level of approximately 1.1 kRU was typically used, giving rise to a maximal response of 10 RU in the interaction analysis and an average apparent surface functionality of >50%. The surface functionality over time was found to be stable, thus not influencing the experiments, in line with previous reports (e.g., ref 20). Although extensive replicates were run, it was difficult to obtain reliable data for some of the compounds at the highest temperatures. These data were excluded from the analysis.

Temperature Dependence of Kinetic Rate Constants and K_D. The interactions between melagatran and the analogues with immobilized thrombin were assessed at seven temperatures, ranging from 5 to 45 °C. A reversible 1:1 interaction model was suitable for description of the data (see the Supporting Information for experimental sensorgrams and fitted theoretical curves). The kinetic rate constants for the different compounds are visualized in a k_{on} versus k_{off} plot (Figure 4) and the temperature dependence of the rate and equilibrium constants in Figure 5. The replicates for the different temperatures showed that the variance of observed k_{on} values was larger than that of the observed k_{off} values (Figure 5). This can be expected as the association event, but not the dissociation event, is affected by ligand concentration.

Because of the very rapid interactions, one needs to interpret the individual data with caution. Nevertheless, it is clear that melagatran had the lowest affinity of all tested compounds, which can be attributed to it having the lowest association rate

dx.doi.org/10.1021/bi301333z | *Biochemistry* 2013, 52, 613–626

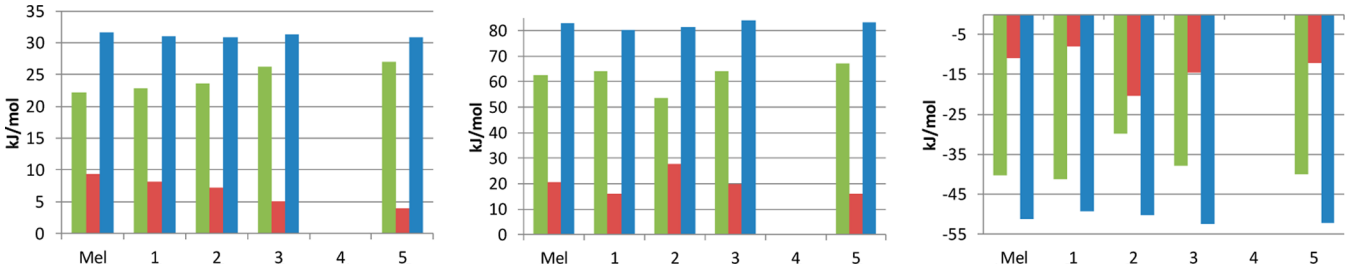

Figure 3. Thermodynamic data from stopped-flow analysis at 25 °C for melagatran and P3 analogues for association, dissociation, and equilibrium (from left to right, respectively): ΔH (green), $-T\Delta S$ (red), and ΔG (blue). Mel stands for melagatran.

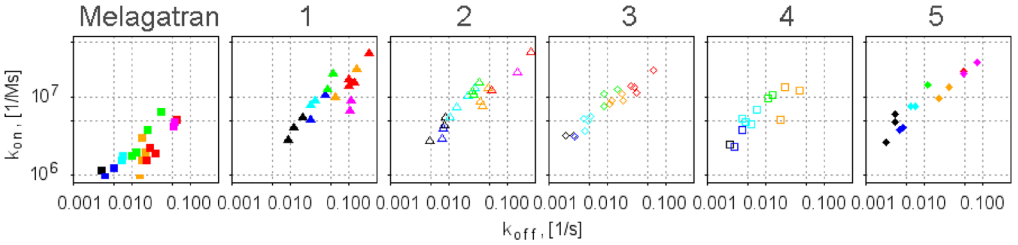

Figure 4. Relationships between k_{on} and k_{off} over a range of temperatures for melagatran and P3 analogues. Data are from SPR biosensor experiments. Black symbols represent data from analysis at 5 °C, blue symbols 10 °C, cyan symbols 15 °C, green symbols 25 °C, orange symbols 35 °C, red symbols 40 °C, and magenta symbols 45 °C.

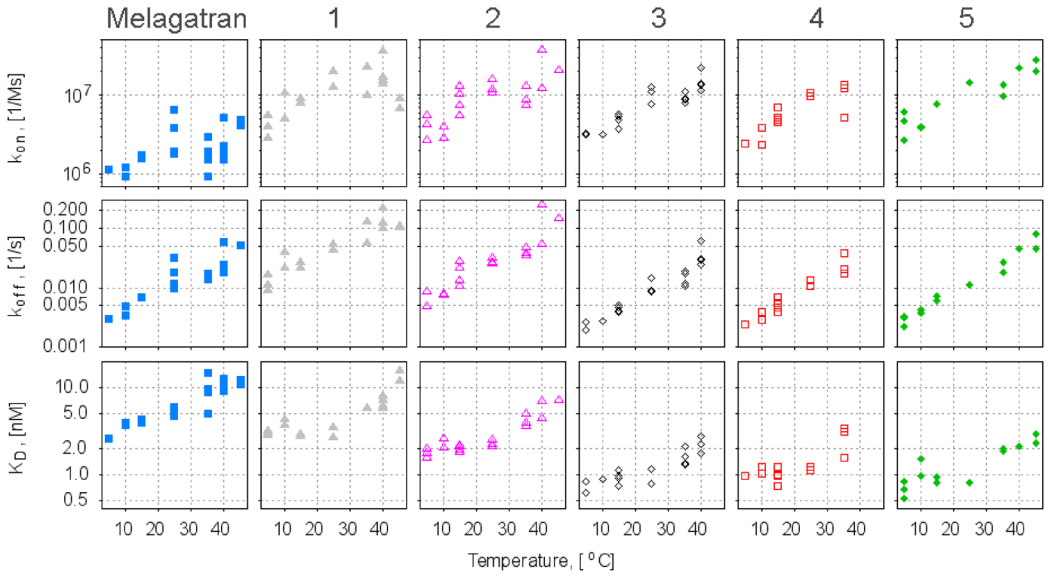

Figure 5. Temperature dependence of (a) association rate constants (k_{on}), (b) dissociation rate constants (k_{off}), and (c) equilibrium constants (K_D), for melagatran and P3 analogues from SPR biosensor experiments.

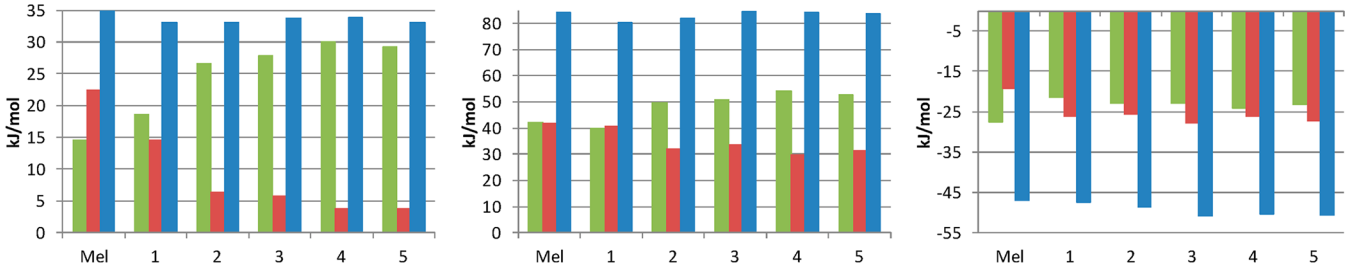

Figure 6. Thermodynamic profiles for melagatran and P3 analogues from SPR biosensor experiments at 25 °C for association, dissociation, and equilibrium (from left to right, respectively): ΔH (green), $-T\Delta S$ (red), and ΔG (blue). Mel stands for melagatran.

constant but a similar dissociation rate constant (Figure 4). The other inhibitors were more similar, and their affinities increased with chain length, primarily an effect of lower dissociation rates for the more aliphatic compounds.

dx.doi.org/10.1021/bi301333z | *Biochemistry* 2013, 52, 613−626

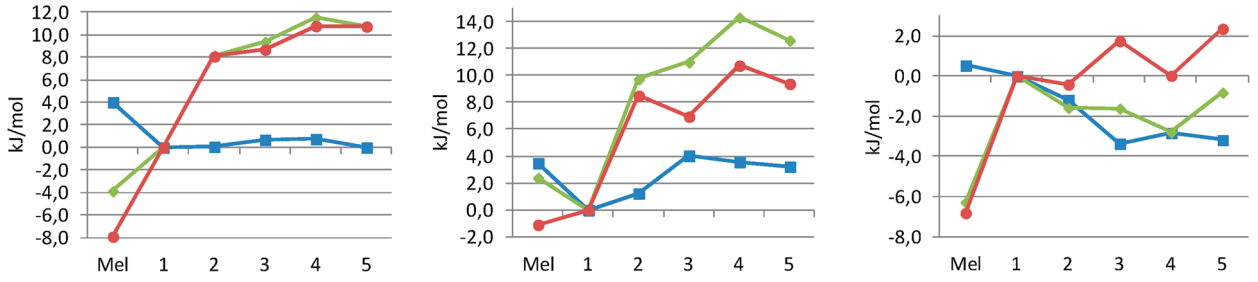

Figure 7. Relative thermodynamic contribution of the P3 side chain for melagatran analogues for association, dissociation, and equilibrium (from left to right, respectively) at 25 °C and as compared to data of inhibitor **1** from SPR interaction analysis through Eyring and van't Hoff analysis: ΔH (green diamonds), $T\Delta S$ (red circles), and ΔG (blue squares).

As anticipated, the kinetic rate constants increased with increasing temperature (Figure 5), but at somewhat different rates and starting points. The propyl-, dimethyl-, ethyl-, and, to some extent, methyl-substituted inhibitors displayed continuously increasing kinetic rate constants with increasing temperature. In contrast, k_{on} for melagatran and the unsubstituted amide was not. This is not believed to be an MT artifact because the ethyl amide-substituted compound proved to be the most prone to giving rise to MT limitations, especially at higher temperatures. The ethyl-substituted inhibitor was therefore only studied in the temperature range of 5−35 °C.

Thermodynamic Analysis. The thermodynamic profiles of the inhibitor series (Figure 6) were established via Eyring and Arrhenius analysis of the association and dissociation events, and van't Hoff analysis of the equilibrium (Supporting Information). However, the larger variance of the association data compared to that of dissociation and equilibrium data should be kept in mind when comparing the data. To assess the relative thermodynamic contributions of the groups in the aliphatic chain, a comparison of the individual thermodynamic parameters with compound **1** was also performed (Figure 7).

These data revealed that association had a dominating enthalpic term that increased with the chain length or degree of substitution. Melagatran displayed a somewhat different profile for the association with a much larger entropic contribution. In contrast, the entropic and enthalpic contributions to dissociation of the melagatran analogues from their target were of similar magnitude for the unsubstituted compound, but the enthalpic contribution increased somewhat with the chain length or degree of substitution. The differences between the different compounds were considerably smaller for the equilibrium constants, indicating that the finer details of the thermodynamic profiles need to be resolved into the association and dissociation events.

ITC Analysis. The calorimetric binding enthalpy of the interaction between the different inhibitors and thrombin was assessed by ITC at four temperatures. This direct method was an important complement to the indirect estimation of the thermodynamic parameters from the temperature dependence of the equilibrium binding constant from SF and SPR biosensor analysis. Furthermore, it allowed for the determination of the heat capacity changes associated with the binding of the tested compounds. All binding isotherms could be described by a 1:1 interaction model (see the Supporting Information for experimental data). The stoichiometry was between 0.97 and 1.01, indicating full activity of the used enzyme. The calorimetric binding enthalpies could be determined with good accuracy, as reflected by the small standard deviations between duplicate measurements. All tested inhibitors experienced a favorable enthalpy of binding. It was influenced by an unusually strong negative heat capacity change of approximately -1.7 kJ mol^{-1} K^{-1}. As a consequence, the binding becomes more exothermic with an increasing temperature. It is noteworthy that, despite the substantial structural differences between the inhibitors, the heat capacity changes were statistically indistinguishable for the different compounds. This implies that the dominating contribution to the heat capacity changes (e.g., expected changes in the solvent accessible surface areas and other ordering parameters as a result of inhibitor binding) originates from the P1 and P2 moieties rather than the P3 residue.

The high affinity of the inhibitors prevented the direct and reliable determination of K_D values and, thus, the free energy of binding. This is reflected by the steep binding isotherms, which became almost rectangular in shape (see the Supporting Information for the experimental data), and the fact that experiments had to be performed under conditions where the Wiseman "*c*" parameter was >1000 (the *c* value is the product of the thrombin concentration and the binding constant K_A).

Because all the inhibitors experienced a similar negative heat capacity change, the relative changes in their enthalpy signatures allowing for the analysis of individual group contributions were essentially similar within the tested temperature range. The analysis could therefore focus on a temperature (35 °C) that had produced a data set with small margins of error, thus allowing the significance of our observations to be assessed. It established that melagatran has the most favorable observed enthalpy of binding for all tested inhibitors (Figure 8a), as already concluded from the SPR biosensor experiments but not SF analysis. In contrast, all P3-substituted melagatran analogues showed a relative reduction in ΔH_{obs}. The effect was strongly dependent on the nature of the substitution. Interestingly, the reduction in ΔH_{obs} did not lead to a reduction in the affinity as shown by the SPR and enzyme inhibition studies, thus pointing toward an increase in the entropic contribution that even overcompensates for the enthalpy loss.

To analyze the impact of the individual group contributions on the binding thermodynamics, compound **1** was taken as a reference (Figure 8b). There is a large difference in the thermodynamic profile between melagatran (carboxylate) and compound **1** (carboxyamide), with a large increase in the negative ΔH_{obs} value of ~7 kJ/mol at 35 °C. Only compound **3** showed a similar but much smaller increase in the enthalpic contribution, whereas compounds **2**, **4**, and **5** show a further reduction in ΔH_{obs}.

As both SPR data and enzyme inhibition studies (SF) show a trend of an increase in affinity that is concomitant with

dx.doi.org/10.1021/bi301333z | *Biochemistry* 2013, 52, 613−626

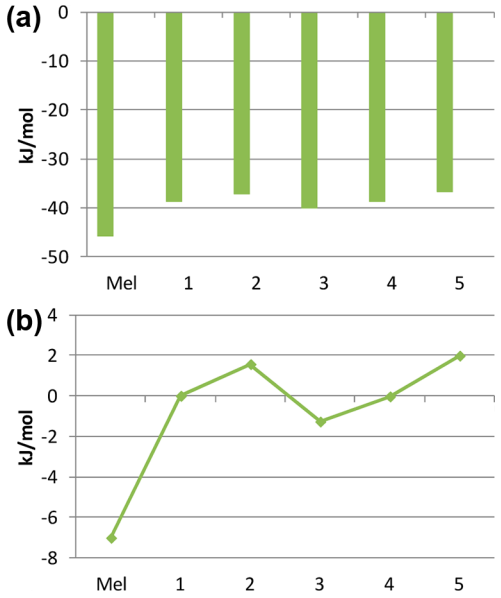

Figure 8. Binding enthalpy signatures of melagatran and P3 analogues determined by ITC at 35 °C. (a) Observed binding enthalpies (ΔH_{obs}) of melagatran and its analogues. (b) Relative group contribution of P3 side chain variations to the overall binding enthalpy using compound **1** as a reference.

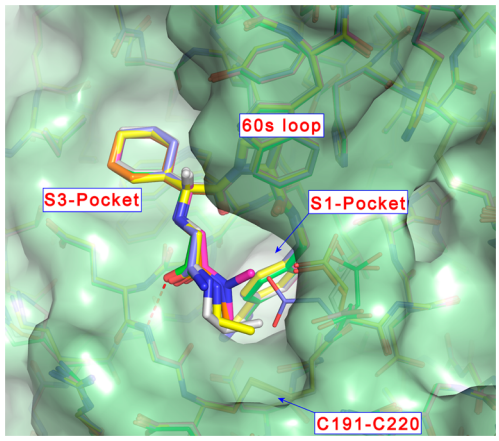

Figure 9. Overlay of the structural complexes between thrombin and melagatran, and the five P3 side chain analogues (with bond models). The surfaces are shown for the melagatran complex. Color coding (carbon atoms) was as follows: green for melagatran, blue for compound **1**, orange for compound **2**, purple for compound **3**, yellow for compound **4**, and gray for compound **5**. S1 and S3 pockets as well as the 60s loop and the C191−C220 disulfide bridge are indicated by boxed text. The S2 pocket is located under the 60s loop.

increasing chain length, it appears that this is a result of the increased entropic contribution. This is manifested in the trend that could be observed for the enthalpic penalty, which develops with increasing chain length. This trend is actually distorted by compound **3**, the tertiary amide, which clearly differed from the other compounds.

Structural Analysis. The structures of the complexes of all six inhibitors with thrombin were determined to ∼1.9 Å [ranging from 1.87 to 1.94 Å (see the Supporting Information for the data collection and refinement statistics)]. The six structures for melagatran and compounds **1**−**5** have been deposited in the Protein Data Bank (entries 4bah, 4bao, 4ban, 4bam, 4baq, and 4bak, respectively). Overall, the data were of good quality in terms of completeness, redundancy, and signal-to-noise ratio (high I/σ and low R_{merge}). The high resolution of the structures allowed the finer details of the interactions, including the position of water molecules, to be seen. The entropic contributions of the ligands in the complexes were estimated from their relative mobilities and calculated from *B* factors as B_{ligand}/B_{site}: 1.26 for melagatran, 1.29 for compound **1**, 1.41 for compound **2**, 1.12 for compound **3**, 1.23 for compound **4**, and 1.41 for compound **5**.[29]

Overview. An overlay figure with all six inhibitor−thrombin complex structures (Figure 9) and the separate illustrations of the individual complexes (Figure 10) show that they only differed significantly around the carboxy or amide end of the P3 groups of the ligand and the Glu192 side chain of the protein. The carboxy/amide plane seems to have a slightly different tilt for the different substitutions, in such a way that the carbonyl oxygen H-bond with Gly219 maintains the same distance (2.9 Å) for all ligands, but with a slightly altered geometry.

The side chain of Glu192 adopted dual conformations in the melagatran complex, while the other compound complexes had only a single orientation for this residue, but with different orientations in the different complexes. Another important difference caused by the minor modifications in the ligand structures was observed as alterations in the solvent structure in the region of the side chain of Glu192. Clearly, the slight perturbations in the orientation of protein side chains as well as the water structure constitute the basis for the observed kinetic and thermodynamic profiles for the ligands.

Comparative Analysis. A comparison of the complexes of melagatran and the amide-substituted ligand (compound **1**) shows that the H-bond to the NH group of Gly219 is maintained from the O of the amide (with a slight tilt in the orientation). However, in the complex with the amide compound, Glu192 is flipped toward the ligand, forming a direct H-bond to the amide nitrogen, resulting in the loss of four solvent positions on both sides of Glu192, as compared to the melagatran complex.

Via addition of a methyl group to the amide (the methyl amide end group), as in compound **2**, the H-bond to the side chain of Glu192 is retained. However, it pushes Glu192 back somewhat toward the position it has in the melagatran complex, but only in a single conformation. It also tilts the methyl−amide plane, but in the opposite direction compared to that of the intact amide. The small effect on Glu192 allows it to regain two of the four solvent positions lost in the carboxy to amide substitution. The added methyl group displaces a water position that was conserved in the melagatran and the amide compound complexes. Overall, the solvent structure in the methyl amide complex is more similar to the melagatran than the amide complex. This illustrates that subtle changes caused by a different substitution of the ligand can propagate the changes to a longer range, resulting in an overall enhanced effect in the binding thermodynamics.

The entropic calculations (see above) indicate that the methyl amide had a stronger entropic signature than the amide compound.[29] After the addition of another methyl group, the dimethyl amide (compound **3**) takes a position identical to that of the methyl amide and pushes Glu192 farther back to its position, as in the melagatran complex though with a single conformation. The H-bond between the ligand and Glu192 seen previously for the methyl amide is no longer present. The overall structure of the solvent around Glu192 is very similar to

dx.doi.org/10.1021/bi301333z | *Biochemistry* 2013, 52, 613−626

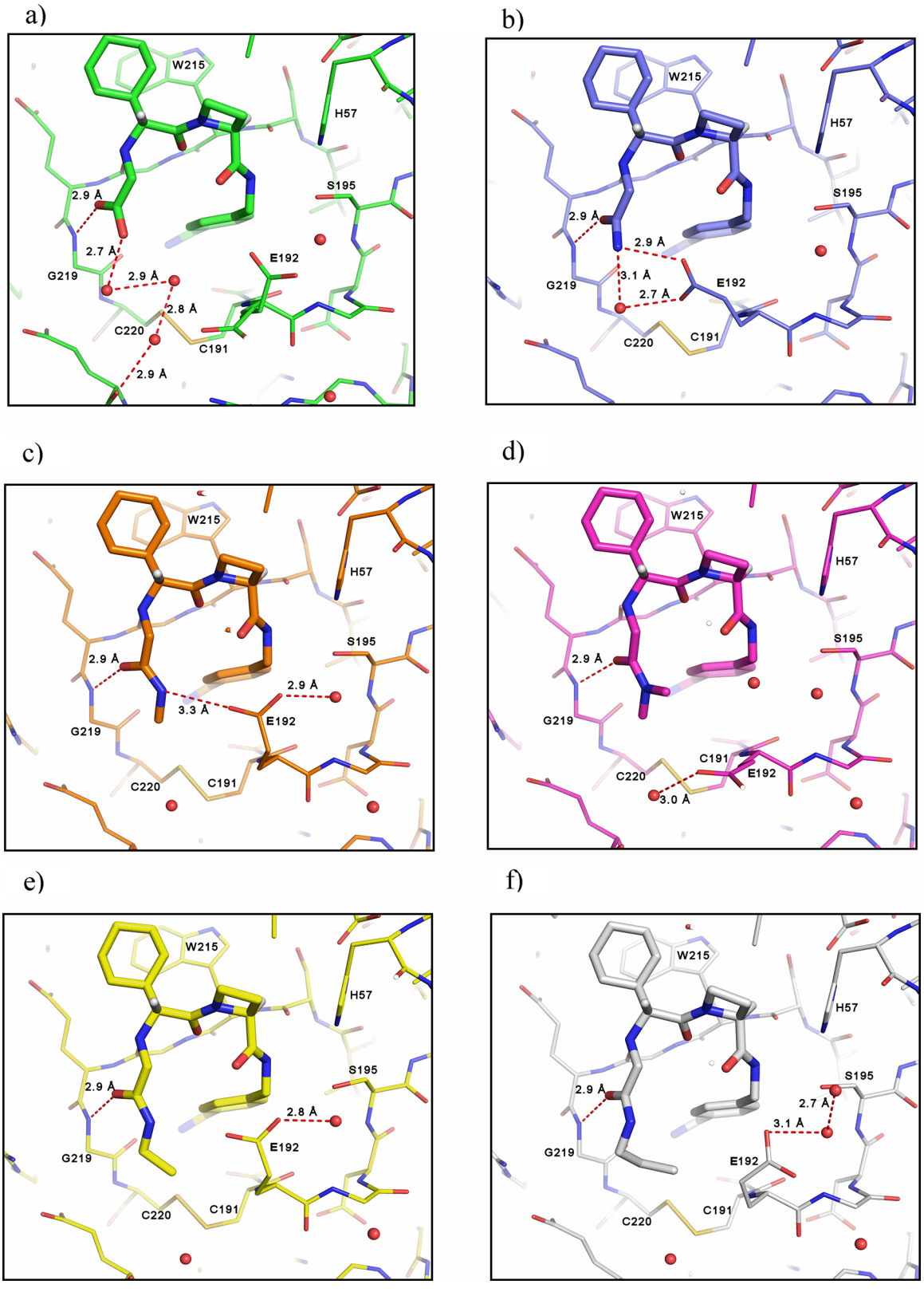

Figure 10. X-ray structures of thrombin in complex with inhibitors. Color coding (carbon atoms) was as follows: green for melagatran, blue for compound **1**, orange foor compound **2**, purple for compound **3**, yellow for compound **4**, and gray for compound **5**. The structures are shown in exactly the same orientation: (a) melagatran (note that the side chain of Glu192 shows dual conformations as in the apo structure), (b) compound **1**, (c) compound **2**, (d) compound **3**, (e) compound **4**, and (f) compound **5**. Hydrogen bonds involving the end group, Glu192, and their neighboring water molecules are indicated as dashed lines. The labeled text indicates the hydrogen bond distances as well as some important protein residues.

that of the methyl compound, except that a water molecule seems to fill the previous position of the side chain of Glu192 in the methyl compound. In addition, the entropic contribution of the bound ligand (B_{ligand}/B_{site}, 1.12) seems to be significantly

dx.doi.org/10.1021/bi301333z | *Biochemistry* 2013, 52, 613−626

smaller than that of the methyl amide (1.41), while we observe an increased ΔH_{obs} term for the dimethyl compound. The dimethyl amide showed the largest change in geometry for the H-bond to the N of Gly219; the O has shifted ~1 Å in a nearly orthogonal direction relative to the H-bond without the distance changing (2.9 Å).

Replacing the methyl with an ethyl group on the amide (compound **4**) does not change the conformation of Glu192. In the H-bond between the ethyl amide and the N of Gly219, the ethyl amide plane tilts back toward that of the intact amide. The extra methyl group clearly affects the solvent positions of the near side of Glu192 because there is a net loss of one water molecule compared to the methyl amide. The entropic contribution of the bound ligand seems to be lower for the ethyl amide than the methyl amide; at the same time, we observe a larger ΔH term for the ethyl amide, thus making the release of the water molecule an enthalpically favored process

Adding a propyl group to the amide (compound **5**) pushes the side chain of Glu192 nearly back to the same position that it occupies in the melagatran complex. The substituted amide plane adopts the same position as the intact amide compound. Despite the larger size compared with that with the ethyl substitution, the solvent structure of the propyl compound complex is similar to that for the methyl compound on both sides of Glu192. In terms of the entropic contribution of the bound ligand, the propyl has the same signature as the methyl substitution, namely similarly high entropic term of the bound ligand and similar ΔH_{obs} terms for the two ligands.

DISCUSSION

Despite a growing awareness in the field of drug discovery of the importance of understanding the kinetics and thermodynamics of drug−target interactions for the selection and optimization of lead compounds, there are surprisingly little experimental data substantiating many of the underlying assumptions. To explore how structural features of ligands translate into kinetics and thermodynamics, we have used a combination of different biophysical methods to generate detailed information about the interaction between inhibitors and their targets.

As a model system, we used thrombin, an important cardiovascular drug target, and a once approved drug, melagatran. To explore the effect of structural variations, we also used a series of P3-substituted analogues of melagatran. The compounds were selected to be representative prototypes of close lead analogues typically synthesized during lead optimization, being potent active site inhibitors with minor differences in their structures. They had K_i and K_D values in the nanomolar range, with k_{on} values exceeding 10^7 M^{-1} s^{-1} and dissociation rates below 0.2 s^{-1}. This challenged the SPR biosensor assay, because many of the interactions were observed to be severely mass transport limited, and thus diffusion-controlled, often not displaying true kinetic behavior. To counter this effect, low surface immobilization levels and high system flow rates were used. Despite these efforts, the interaction data were often found to be in the MT twilight zone. Because trends in data were sought, a less stringent MT threshold was used. Although it might also be that the inhibition kinetics from the SF data have been compromised by the rapid interactions, this is not immediately obvious from the data. However, by using these three complementary techniques, limitations in one method or another can be detected and included in the analysis. For example, the used SF analysis was indirect and made use of inhibition of product formation from a substrate and analysis of the catalytic reaction, while SPR analysis, which directly monitors the interaction between the inhibitors and the enzyme, has the potential disadvantage of immobilization of one of the binding partners. An alternative for the used stopped-flow absorbance spectroscopy might be the stopped-flow fluorescence spectroscopy, based on conformational changes in the enzyme upon ligand binding, as previously used.[10] SF and SPR methods have the advantage of being time-resolved, allowing the measurement of rate constants, whereas ITC measures only at equilibrium, although it directly monitors enthalpy, a parameter that is obtained only indirectly by the other methods.

Kinetic Analysis. Stopped-flow analysis was initially used as a functional assay to evaluate the inhibitory and kinetic properties of the compounds. Because the inhibitory potencies of these compounds were rather similar, and the differences in the rate constants were minor, it was not possible to conclusively establish the effect of changing the length of the side chain on the inhibition. Nevertheless, the method showed that both the degree of substitution of the amide and the length of the aliphatic substituent were clearly influential. (1) The higher the degree of substitution on the amide, the higher the affinity of the inhibitor for thrombin, in the following order: primary ≫ secondary ≫ tertiary. The same trend was seen in the dissociation rate, with the tertiary amide having the lowest k_{off} value. (2) The length of an aliphatic alkyl substituent also affects the inhibition constant, going from highest to lowest as follows: **1** ≫ **2** ≫ **4** < **5**. Again, the same trend was seen in the rate of dissociation, with the ethyl substituent (compound **3**) showing the smallest k_{off} value. There was no discernible trend in the association rates. This may be attributed to the larger errors in the determination of k_{on} than in k_{off}, which is in the nature of the evaluation procedure for which the concentration of the substrate and the K_m are crucial, which are of no importance for the evaluation of k_{off}.

As an alternative, the affinities and kinetic rate constants were also determined by use of SPR biosensor technology. The overall results from the SF measurements and the SPR-based interaction analysis were qualitatively in good agreement, identifying the same trends in inhibitor binding characteristics as a function of the degree of amide substitution and the size of the aliphatic alkyl groups. Melagatran exhibited the lowest affinity, and the affinities increased with an increasing degree of substitution as well as chain length. This could be traced to a corresponding decrease in the dissociation rate for the melagatran analogues; melagatran had an intermediate dissociation rate. The association rates were rather similar for the melagatran analogues, while melagatran had the slowest association rate.

Thermodynamic Analysis. The binding enthalpy profiles of the different inhibitors were quite different. However, the data from SF analysis supported the SPR values, although they were performed with a slightly different experimental design. For example, the SF analysis was performed in a 20 °C interval, between 17 and 37 °C, whereas the SPR measurements were taken in a 40 °C range, from 5 to 45 °C. This difference may be critical because the determination of enthalpies and entropies via linear regression involves estimation of slopes and the extrapolated ordinate intercepts. The accuracy of this procedure is dependent on high-quality data over a large temperature interval,[23] but these conditions are rarely fulfilled with proteins.

Unfortunately, the affinities could not be determined from the ITC data because of steep binding isotherms, although this problem is often addressed by displacement titrations, which involves the artificial lowering of the measurable association binding constant via premixing of the target protein with a weaker competitive ligand. As this requires the determination of the full thermodynamic profile of the weaker ligand for the calculation of the binding parameters of the high-affinity ligand, this procedure will introduce larger errors due to error propagation and in particular affect the statistical significance of the entropy parameters. Even though SPR data could also have been potentially used in combining them into a full thermodynamic profile of the inhibitors and thereby determining their entropic signatures, there is the caveat that a K_D value from an ITC experiment is not necessarily the same as a k_{off}/k_{on} ratio from SPR. This would obviously introduce inaccuracies and lead to erroneous conclusions when interpreting the thermodynamic profiles. In summary, we deliberately made no attempts to use displacement experiments or to apply the K_D data from the SPR experiments for entropy calculations but focused instead solely on the analysis of the observed binding enthalpy (ΔH_{obs}) for our interpretations and conclusions.

The most evident thermodynamic differences between the SF- and SPR biosensor-derived data are the contributions of enthalpy and entropy to the Gibbs free energy. For SF, the enthalpy of dissociation, $\Delta H^{\ddagger}_{off}$, contributed to most of the Gibbs free energy, $\Delta G^{\ddagger}_{off}$, without a clear trend for the different inhibitors. In contrast, the SPR data showed similar figures of entalpic and entropic terms and a clear trend where melagatran and the unsubstituted amide had equal contributions of enthalpy and entropy, while the enthalpic term increased with chain length. Both methods found that the enthalpic contribution to k_{on} increased with chain length. The contributions of entropy and enthalpy were similar for melagatran and the unsubstituted amide when measured by SPR, but they were dominated by enthalpy in the SF data. It is not clear why the different methods give these differences, but the methods do record somewhat different parameters of the system and can result in slight differences when translated into thermodynamic terms. Nevertheless, it translates to rather large differences in the equilibrium, where the SPR data suggest that all compounds have a balanced contribution of enthalpy and entropy to the Gibbs free energy, with a clear trend for the analogues. The SF method shows a dominant enthalpy but no clear trend.

Despite the unusually large heat capacity change, the ΔH_{obs} data measured directly by ITC at 25 °C matched the calculated enthalpy values derived from the SPR data. This cannot readily be assumed because the indirect analysis using a temperature series can potentially be influenced by temperature-dependent processes not relating to the interaction as such, while the direct determination of enthalpies via calorimetric studies is not affected by such secondary effects. The ITC experiments thus confirmed that melagatran had the most enthalpy-dominated binding equilibrium. The same effects of the degree of substitution and increased chain length were also seen for this approach, thus highlighting the possibility of deriving reliable binding enthalpy values from affinity data despite a large negative heat capacity change caused by the binding of the compound.

Structural Interpretation. The structures of the complexes revealed that the minor structural differences in the inhibitor series resulted in significant changes in the orientation of one of the side chains in the protein (Glu192) and the water structure. An H-bond between the oxygen in the substituted group and the backbone of Gly219 was maintained for all the compounds. This contributed to the preservation of the same orientation of the inhibitors in the binding site, facilitating the structural interpretation. However, there are two distinct structural features of the inhibitors in the current series, making them more or less effective as thrombin inhibitors. The first feature is related to the amide hydrogen present in all melagatran analogues except the tertiary amide. For compounds **1**, **2**, and **4**, but not compound **5**, it appears to form an H-bond with Glu192. Melagatran lacks this group but has a carboxylate group instead, which appears to interact with Glu192 via two bridging water molecules, contributing to the fact that its characteristics deviate even more greatly than those of the tertiary amide. The second feature is the hydrophobic interaction between nonpolar P3 substituents and the hydrophobic area ("cleft") between Trp60D and the Cys191–Cys220 disulfide bridge. These features influence both the kinetics and the thermodynamics of the interactions, as outlined below.

Structural–Kinetic Relationships. The interaction between the amide hydrogen and Glu192 is expected to play a part in both association and dissociation processes. However, on the basis of the SPR biosensor data, there is no significant difference seen in the kinetics between the tertiary amide and the other melagatran analogues, indicating that this interaction does not contribute significantly to the kinetics of either association or dissociation. In contrast, the relatively slow association of melagatran can be attributed to its carboxylate moiety, which appears to electrostatically repel the carboxylate group of Glu192. This is seen in the two orientations of the Glu192 residue, both clearly shying away from the melagatran carboxylate.

The effects of these hydrophobic interactions are most evident for the dissociation process in which a longer, and thereby more hydrophobic, hydrocarbon chain yields a slower k_{off}. However, there is little difference in k_{off} among compounds **3**–**5**, indicating that there is a size limit after which there is no additional advantage. It can be interpreted in terms of creating the smallest possible solvent accessible area in the crevice between the loop regions and thereby shielding off the amide hydrogen from interaction with the solvent, thus resulting in a lower k_{off}. Another feature that could influence the structural–kinetic relationship is the effect of alkyl substituents on the surface water network, as has recently been shown for another set of inhibitors and thrombin.[30]

Structural–Thermodynamic Relationships. The explanation for the difference in the distribution of enthalpy can be derived from the number of intermolecular interactions that have to be broken during the dissociation process of the inhibitor from thrombin. The difference in the distribution of entropy is more complex and not so easily explained but can to some extent be derived from the solvent effect of the water molecules surrounding the species involved in the interaction or from a specific intramolecular hydrophobic interaction leading to a "hydrophobic collapse" as has been observed for argatroban,[31] another thrombin inhibitor.

The amide hydrogen appeared to reduce the enthalpic contribution of the binding equilibrium. The ITC data (Figure 8b) showed that the dimethyl substitution provided the largest enthalpy contribution in the analogue series. This could be attributed to the absence of an amide proton that needs to be

dx.doi.org/10.1021/bi301333z | *Biochemistry* 2013, 52, 613–626

desolvated, which in all other melagatran analogues is involved in the formation of a hydrogen bond with the Glu192 side chain. Because melagatran, having a hydroxyl group instead of an amide, had the largest enthalpic change, there may be other reasons in addition to desolvation that make these compound analogues differ. To better understand this, as an example, an extended comparison is made between the congeneric pair melagatran and compound **1** that differ structurally only by the small substitution of a hydroxyl group with an amine group.

Unexpectedly, compound **1**, which experiences a reduced negative ΔH_{obs} value, forms an additional hydrogen bond to Glu192 that is not present in the melagatran complex. This is achieved via a significant shift in the Glu192 side chain position that points toward compound **1**. Still, the H-bond to the backbone amide of Gly219 and the carbonyl of compound **1** is maintained as well as all other key interactions. This raises the question of the origin of this reduced negative ΔH_{obs} value, as additional hydrogen bond formation is generally reflected by increased negative ΔH_{obs} values. First of all, some price in energy has to be paid to orient the Glu192 side chain toward the compound to allow the buildup of the additional hydrogen bond. Furthermore, the carboxylate of the melagatran is partially charged, thus making the existing hydrogen bond with the backbone amide of Gly219 particularly strong. The introduction of the amine group will thus weaken this maintained hydrogen bond and consequently reduce the binding enthalpy originating from that interaction. Finally, the associated desolvation enthalpies for the Glu192 carboxylate as well as the carboxyamide of compound **1** will also lead to a further reduction in the observed binding enthalpy. All the described effects will synergistically lead to an overall reduction in the enthalpic contribution to offset the expected increase in enthalpy from the additional hydrogen bond formation. Nevertheless, the affinity remains almost unchanged, which can be attributed to the dramatic change in the water molecule inventory in the proximity of Glu192. The additional hydrogen bond formation leads to a loss of four solvent positions, thus increasing the entropy favorably. This obviously exceeds substantially the entropic penalty resulting from the considerable loss of the degree of freedom of the Glu192 side chain.

The heat capacity change observed by ITC did not change with the size of the P3 substituent and, thus, the solvent accessible surface area (SASA). In other words, the entropy-driven affinity increase was not reflected in the heat capacity change. Future studies could therefore be aimed at structure−activity relationships with compounds involving more hydrophilic residues or aromatic rings as amide substituents.

While this paper was being prepared, a thermodynamic investigation of more bulky, hydrophobic P3 substituents from two different, melagatran-unrelated compound series has been presented and discussed.[30] The hydrophobic P3 substituents impact directly the solvation state in the S3−S4 pocket and follow the pattern of a classical hydrophobic effect, as also indicated in this study. The observed pattern is characterized by an increase in the entropic contribution coinciding with the displacement of water molecules and the formation of van der Waals contacts as the substituents become more bulky. As the experiments were conducted at a single temperature, a further extension of such measurements toward the determination of the associated heat capacity changes could allow a deeper characterization of the observed entropy changes as attempted in this study.

Consequences of Applying Kinetic and Thermodynamic Data for Drug Design. The last couple of years have seen an increased demand particularly from medicinal chemists to apply kinetic and thermodynamic data more often in early drug discovery to support the search for kinetic and thermodynamic signatures within lead series. Connected to this are the expectations that through stronger consideration of such data during the early phases of hit discovery and drug design one is able to address some late stage key issues of current drug discovery relating merely to safety and efficacy. These expectations are further fueled by the growing ability to produce such data on an increasing number of targets and compounds with timelines that are compatible with the early drug discovery process.

This study highlights elegantly the challenge of using kinetic and thermodynamic data as a sole driver for identifying compounds with good lead properties or using such data for rational, prospective drug design. We have been unable to observe a clear trend for the binding enthalpy of a compound and its binding kinetics or inhibitory potential. The lack of correlation is actually not unexpected in light of the structural data we have presented in this study, as both small structural rearrangements within the protein binding site and subtle changes in the relative orientation of the compounds as well as changes in the local water structure are leading to unpredictable consequences for the kinetic and thermodynamic signatures. In the context of prospective drug design, a particular emphasis is placed on the binding enthalpy as a direct measure of the net change in the number and/or strength of the noncovalent bonds on going from the free to the bound state. This obviously goes beyond hydrogen bond formation and/or dipole−dipole interactions as it also involves processes like ligand desolvation, rearrangement of local water structures, and structural adaptation of ligand and protein that are hard to decompose into their individual enthalpy contributions. To highlight this particular challenge, we have, for example, observed a loss of binding enthalpy upon hydrogen bond formation and a small but significant gain in the binding enthalpy upon breakage of a hydrogen bond. On first sight, this is counterintuitive, but it is actually not surprising given the totality of the involved processes having different impacts on the overall net change in enthalpy. This highlights the risk in using either kinetic or thermodynamic information in isolation without consideration of structural information that eventually exists or might become available for a given protein−ligand complex. This is particularly important during the analysis of close compound analogues as outlined in this work, as one of the main prerequisites for an appropriate analysis of individual group contributions (matched pair analysis) in the absence of structural information is the unperturbed and conserved binding mode of the parental compound as well as a maintained local water structure and a similar burial of solvent accessible surface area. Small adjustments in ligand orientation that could originate from the accommodation of the introduced substituents or changes in the local water inventory will have additional kinetic and thermodynamic consequences that cannot be correctly interpreted without structural data at hand. To add to the complexity of the challenge, an unaffected kinetic or thermodynamic signature is not a reliable indicator of a conserved binding mode either, which is one of the conclusions from a recent study involving P3-substituted thrombin inhibitors.[30]Ultimately, this is further complicated by small but critical changes in the water structures of the

different protein−ligand complexes as seen in this as well as other recent studies.

A larger number of melagatran analogues might help to further establish the presence of a kinetic or thermodynamic response. This clearly needs to be underpinned with structural data to relate the kinetic and thermodynamic responses of the system to the buildup of molecular interactions.

CONCLUSIONS

This study has shown that a combination of different biophysical techniques is useful for providing experimental data for interpreting the kinetic and thermodynamic features of interactions from a structural perspective. SPR biosensor technology has an advantage of being both time-resolved and direct, i.e., does not require a substrate, as the SF method does. ITC is superior for determining equilibrium-based thermodynamic parameters, although the high affinity of the current compounds reduced the information content.

The data have revealed that minor changes in the structure of a lead compound can have significant effects on its interaction with the target with direct consequences for the kinetics and thermodynamics of the interaction. In contrast to what may be intuitively expected, additional hydrogen bonding is not necessarily reflected in enthalpy gains, highlighting the impact of differences in the residual solvation structure as well as residual mobility contributions involving the protein and ligand. The strength of kinetic and thermodynamic data is greatest if used in conjunction with structural data.

ASSOCIATED CONTENT

Supporting Information

Additional background experimental data. This material is available free of charge via the Internet at http://pubs.acs.org.

AUTHOR INFORMATION

Corresponding Author

*E-mail: helena.danielson@kemi.uu.se. Phone: +46 18 4714545.

Present Address

[‖]Merck KGaA, Merck Serono Research, Small Molecule Platform, Darmstadt, Germany.

Funding

This work was supported by the Swedish Research Council (UHD).

Notes

The authors declare no competing financial interest.

ACKNOWLEDGMENTS

We thank Ingemar Nilsson for initial contributions to the project and constructive feedback on the content and form of the manuscript.

ABBREVIATIONS

BSA, bovine serum albumin; DMSO, dimethyl sulfoxide; EDC, *N*-ethyl-*N*′-[3-(dimethylamino)propyl]carbodiimide; HEPES, 2-[4-(2-hydroxyethyl)-1-piperazinyl]ethanesulfonic acid; ITC, isothermal microcalorimetry; MT, mass transport; NHS, *N*-hydroxysuccinimide; RU, response units; pNA, *p*-nitroaniline; RB, running buffer; S-2238, H-D-phenylalanyl-L-pipecolyl-L-arginine-*p*-nitroaniline dihydrochloride; SF, stopped-flow; SPR, surface plasmon resonance; Tris, tris(hydroxymethyl)-aminomethane.

REFERENCES

(1) Copeland, R. A., Pompliano, D. L., and Meek, T. D. (2006) Drug-target residence time and its implications for lead optimization. *Nat. Rev. Drug Discovery 5*, 730−739.

(2) Freire, E. (2008) Do enthalpy and entropy distinguish first in class from best in class? *Drug Discovery Today 13*, 869−874.

(3) Gallwitz, M., Enoksson, M., Thorpe, M., and Hellman, L. (2012) The extended cleavage specificity of human thrombin. *PLoS One 7*, e31756.

(4) Schechter, I., and Berger, A. (1967) On the size of the active site in proteases. I. Papain. *Biochem. Biophys. Res. Commun. 27*, 157−162.

(5) Elg, M., Gustafsson, D., and Deinum, J. (1997) The importance of enzyme inhibition kinetics for the effect of thrombin inhibitors in a rat model of arterial thrombosis. *Thromb. Haemostasis 78*, 1286−1292.

(6) Stubbs, M. T., and Bode, W. (1993) A player of many parts: The spotlight falls on thrombin's structure. *Thromb. Res. 69*, 1−58.

(7) Deinum, J., Gustavsson, L., Gyzander, E., Kullman-Magnusson, M., Edström, Å., and Karlsson, R. (2002) A Thermodynamic Characterization of the Binding of Thrombin Inhibitors to Human Thrombin, Combining Biosensor Technology, Stopped-Flow Spectrophotometry, and Microcalorimetry. *Anal. Biochem. 300*, 152−162.

(8) Deinum, J., Mattsson, C., Inghardt, T., and Elg, M. (2009) Biochemical and pharmacological effects of the direct thrombin inhibitor AR-H067637. *Thromb. Haemostasis 101*, 1051−1059.

(9) Gustafsson, D., Antonsson, T., Bylund, R., Eriksson, U., Gyzander, E., Nilsson, I., Elg, M., Mattsson, C., Deinum, J., Pehrsson, S., Karlsson, O., Nilsson, A., and Sorensen, H. (1998) Effects of melagatran, a new low-molecular-weight thrombin inhibitor, on thrombin and fibrinolytic enzymes. *Thromb. Haemostasis 79*, 110−118.

(10) Nilsson, T., Sjöling-Ericksson, Å., and Deinum, J. (1998) The Mechanism of Binding of Low-Molecular-Weight Active Site Inhibitors to Human α-Thrombin. *J. Enzyme Inhib. Med. Chem. 13*, 11−29.

(11) Deinum, J., Gyzander, E., and Gustavsson, L. (2003) Characterization of the interaction of α-thrombin with melagatran analogues with different P3 substituents: a kinetic and thermodynamic study. *J. Thromb. Haemostasis*, Abstract P0032.

(12) Hanessian, S., Therrien, E., Zhang, J., Otterlo, W. v., Xue, Y., Gustafsson, D., Nilsson, I., and Fjellström, O. (2009) From natural products to achiral drug prototypes: Potent thrombin inhibitors based on P2/P3 dihydropyrid-2-one core motifs. *Bioorg. Med. Chem. Lett. 19*, 5429−5432.

(13) Nilsson, M., Hämäläinen, M., Ivarsson, M., Gottfries, J., Xue, Y., Hansson, S., Isaksson, R., and Fex, T. (2009) Compounds Binding to the S2−S3 Pockets of Thrombin. *J. Med. Chem. 52*, 2708−2715.

(14) Fenton, J. W., II, Fasco, M. J., and Stackrow, A. B. (1977) Human thrombins. Production, evaluation, and properties of α-thrombin. *J. Biol. Chem. 252*, 3587−3598.

(15) Dang, Q. D., and Di Cera, E. (1994) A simple activity assay for thrombin and hirudin. *J. Protein Chem. 13*, 367−373.

(16) Pliska, V., and Charton, M. (1991) Antagonists as "affinity probes" for peptide hormone receptors: QSAR studies on oxytocin receptor in the rat myometrium. *J. Recept. Res. 11*, 59−78.

(17) Good, N. E., Winget, G. D., Winter, W., Connolly, T. N., Izawa, S., and Singh, R. M. (1966) Hydrogen ion buffers for biological research. *Biochemistry 5*, 467−477.

(18) Lottenberg, R., Hall, J. A., Blinder, M., Binder, E. P., and Jackson, C. M. (1983) The action of thrombin on peptide p-nitroanilide substrates. Substrate selectivity and examination of hydrolysis under different reaction conditions. *Biochim. Biophys. Acta 742*, 539−557.

(19) Karlsson, R., Kullman-Magnusson, M., Hamalainen, M. D., Remaeus, A., Andersson, K., Borg, P., Gyzander, E., and Deinum, J. (2000) Biosensor analysis of drug-target interactions: Direct and competitive binding assays for investigation of interactions between thrombin and thrombin inhibitors. *Anal. Biochem. 278*, 1−13.

(20) Karlsson, R. (1999) Affinity analysis of non-steady-state data obtained under mass transport limited conditions using BIAcore technology. *J. Mol. Recognit. 12*, 285−292.
(21) Shuman, C. F., Hamalainen, M. D., and Danielson, U. H. (2004) Kinetic and thermodynamic characterization of HIV-1 protease inhibitors. *J. Mol. Recognit. 17*, 106−119.
(22) Geitmann, M., and Danielson, U. H. (2007) Additional level of information about complex interaction between non-nucleoside inhibitor and HIV-1 reverse transcriptase using biosensor-based thermodynamic analysis. *Bioorg. Med. Chem. 15*, 7344−7354.
(23) Cornish-Bowden, A. (2002) Enthalpy-entropy compensation: A phantom phenomenon. *J. Biosci. 27*, 121−126.
(24) Dullweber, F., Stubbs, M. T., Musil, D., Sturzebecher, J., and Klebe, G. (2001) Factorising ligand affinity: A combined thermodynamic and crystallographic study of trypsin and thrombin inhibition. *J. Mol. Biol. 313*, 593−614.
(25) Kabsch, W. (2010) Xds. *Acta Crystallogr. D66*, 125−132.
(26) Collaborative Computational Project, Number 4 (1994) The CCP4 suite: Programs for protein crystallography. *Acta Crystallogr. D50*, 760−763.
(27) Bricogne, G., Blanc, E., Brandl, M., Flensburg, C., Keller, P., Paciorek, W., Roversi, P., Smart, O. S., Vonrhein, C., and Womack, T. O. (2009) *BUSTER*, version 2.11.1, Global Phasing Ltd., Cambridge, United Kingdom.
(28) Emsley, P., and Cowtan, K. (2004) Coot: Model-building tools for molecular graphics. *Acta Crystallogr. D60*, 2126−2132.
(29) Baum, B., Mohamed, M., Zayed, M., Gerlach, C., Heine, A., Hangauer, D., and Klebe, G. (2009) More than a simple lipophilic contact: A detailed thermodynamic analysis of nonbasic residues in the s1 pocket of thrombin. *J. Mol. Biol. 390*, 56−69.
(30) Biela, A., Sielaff, F., Terwesten, F., Heine, A., Steinmetzer, T., and Klebe, G. (2012) Ligand binding stepwise disrupts water network in thrombin: Enthalpic and entropic changes reveal classical hydrophobic effect. *J. Med. Chem. 55*, 6094−6110.
(31) Tucker, T. J., Lumma, W. C., Mulichak, A. M., Chen, Z., Naylor-Olsen, A. M., Lewis, S. D., Lucas, R., Freidinger, R. M., and Kuo, L. C. (1997) Design of Highly Potent Noncovalent Thrombin Inhibitors That Utilize a Novel Lipophilic Binding Pocket in the Thrombin Active Site. *J. Med. Chem. 40*, 830−832.